Supplementary Information for

Dual-nanograting Perovskite Structures for Photodetectors with Enhanced Light Trapping.

Rui Wei, Hongyi Zhao, Qiyang Wang, Jiren Liang, Mingzhong Lv, Weiting Weng and Shun-Xin Li*

State Key Laboratory of High Pressure and Superhard Materials，College of Physics Jilin University，Changchun 130012, China

*Corresponding authors.

E-mail: shunxin2021@jlu.edu.cn

Experimental Section

PDMS template preparation: A mixture of PDMS prepolymer and curing agent at a 10:1 ratio was spin-coated onto the treated commercial optical disc and then heated at 90 °C for 90 mins to obtain the micro-structured PDMS template.

Fabrication of Dual-nanograting crystals and photodetectors: The $MAPbBr_3$, precursor was obtained by mixing MABr and $PbBr_2$, in dimethylformamide (DMF) with an equimolar proportion. The solution was stirred at 60°C for 12 hours. 1 μL droplet of the solution was dispensed onto the treated PDMS, followed by heating at 60 °C for 2 h. Subsequently, the as-prepared Dual-nanograting crystals were fixed onto the laser-etched ITO glass substrates to fabricate photodetectors.

Numerical Simulations: FDTD simulations were performed to model the time-averaged electromagnetic energy distribution using a 3D unit cell with periodic boundary conditions.

Characterization: A field-emission scanning electron microscope (SEM, HITACHI Regulus8100, Japan) was used to characterize the morphology and size of the MAPbBr3 Dual-nanograting crystal and the Planar reference crystal, and energy dispersive spectroscopy (EDS) characterization was conducted using the energy spectrometer that accompanies the SEM. The micromorphology and lattice fringes of the two structures were observed by transmission electron microscope (TEM, JEM-2200FS, JEOL, Japan). The BRUKER-D8 X-ray diffractometer (XRD, Bruker, Germany) was used for the Dual-nanograting crystal and Planar reference crystal s crystallinity with Cu Kα as the target material. The source meter (2636B, Keithley, USA) served as a voltage source and recorded the current variation data.

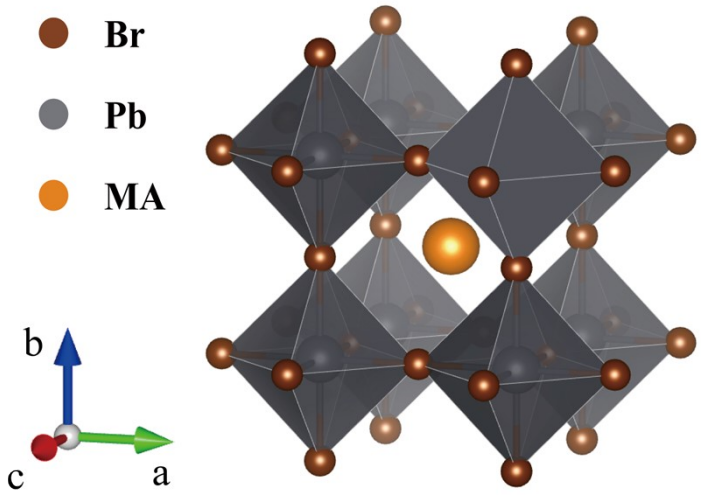

Fig. S1. Methylammonium lead bromide ($MAPbBr_3$) crystal structure.

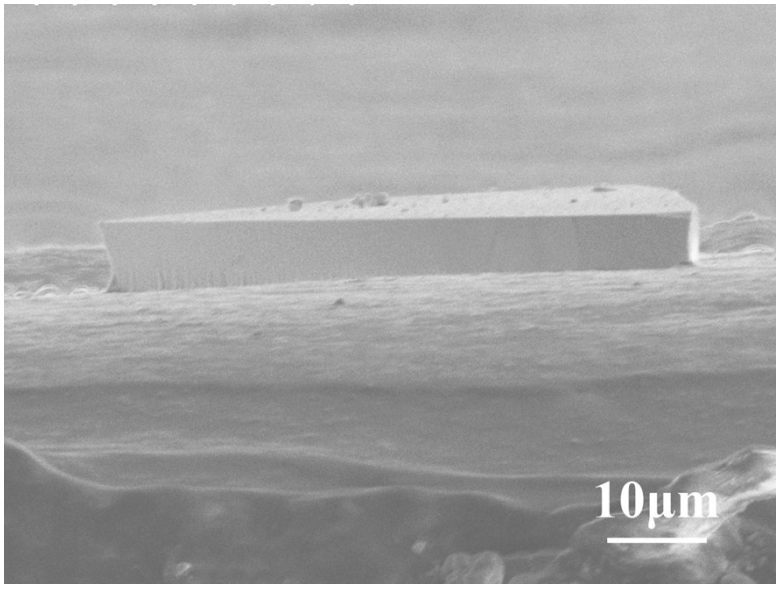

Fig. S2. SEM image of the Planar reference.

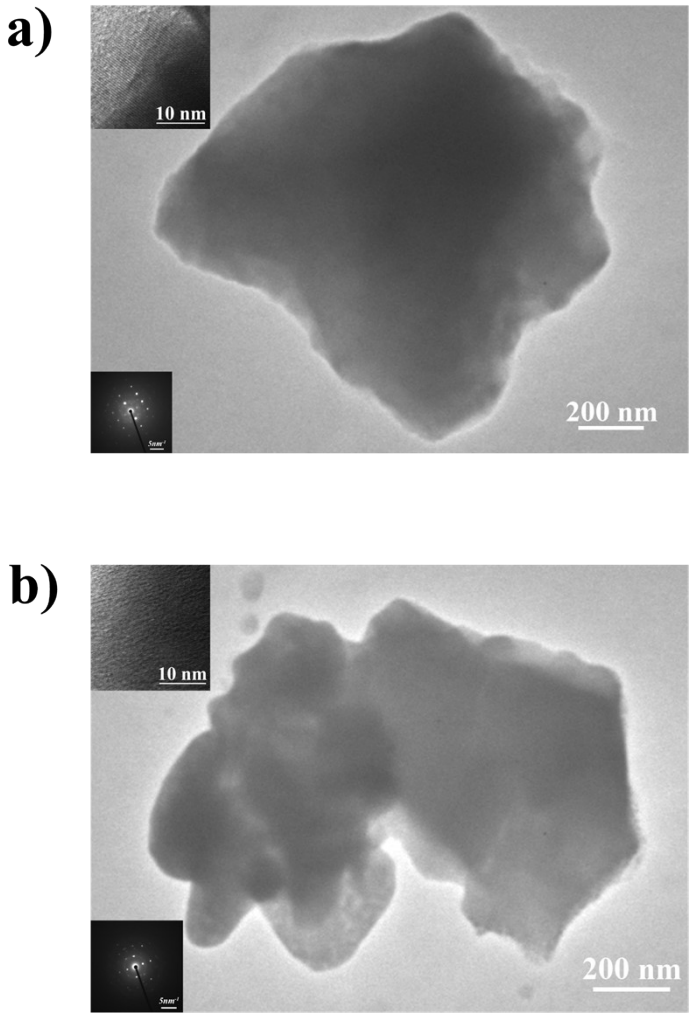

Fig. S3. Microstructural characterization of the Dual-nanograting crystal and Planar reference crystal. (a) TEM image of the double-grating structure. The insets in the top-left and bottom-left corners show the high-resolution TEM (HRTEM) image and the SAED pattern, respectively. (b) TEM image of the Planar reference structure. The top-left and bottom-left insets display the HRTEM image and SAED pattern, respectively.

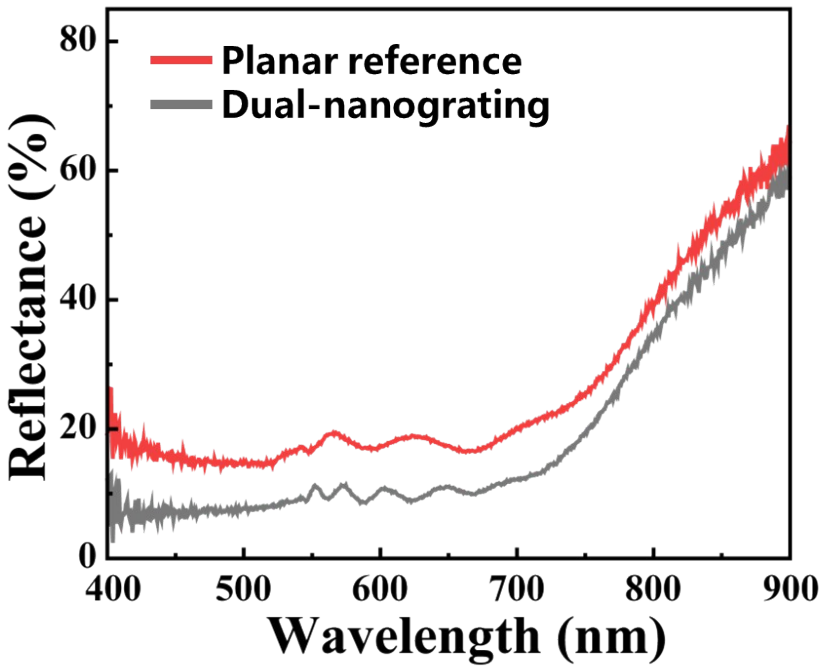

Fig. S4. Absorption spectra comparing the Dual-nanograting with the Planar reference.

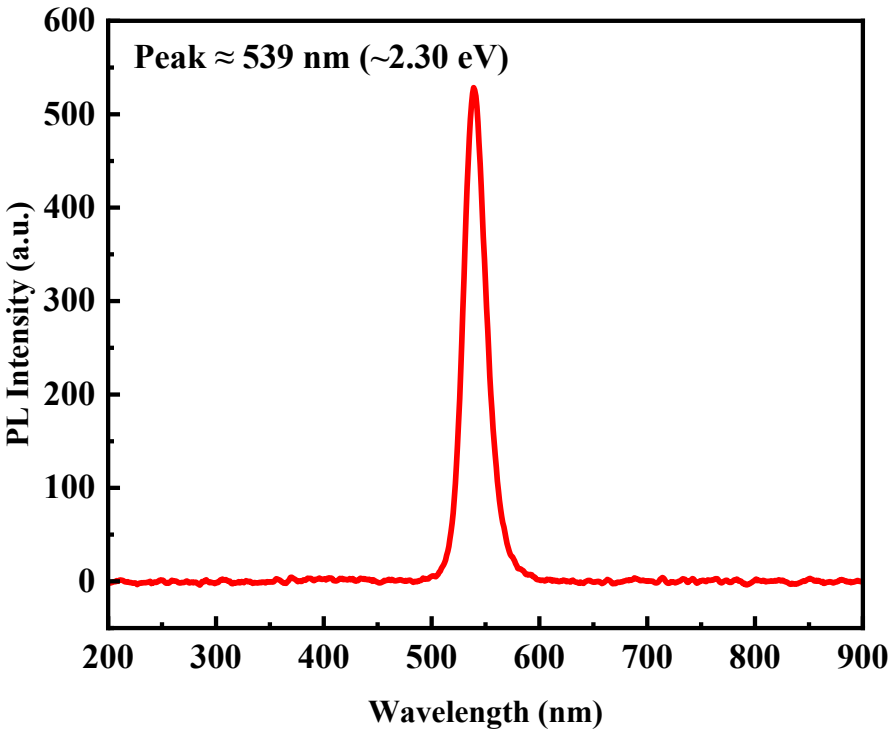

Fig. S5.PL spectrum of the $MAPbBr_3$ crystal, showing a dominant emission peak at 539 nm (≈ 2.30 eV).

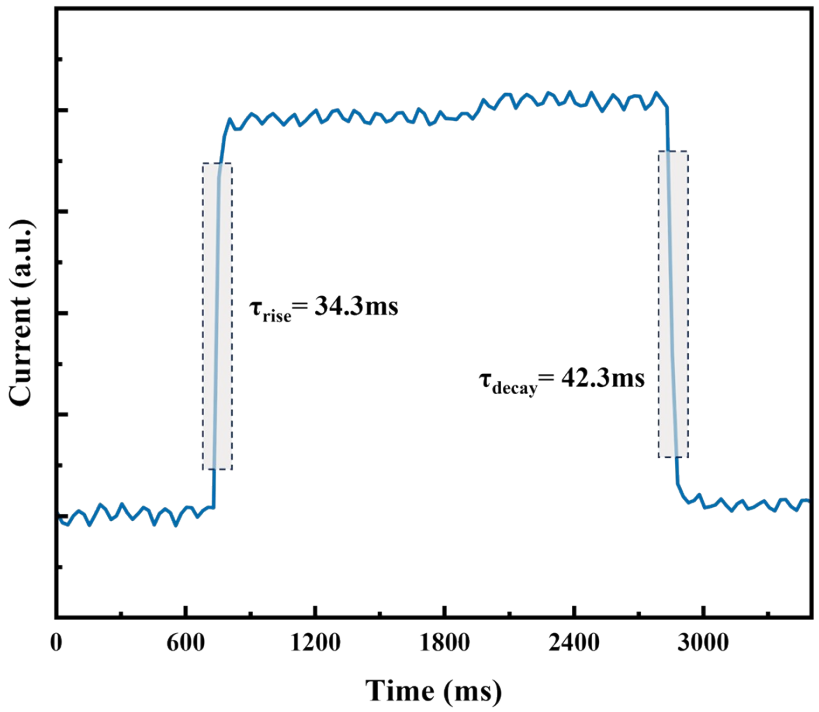

Fig. S6. Response time of the Dual-nanograting structured PDs.

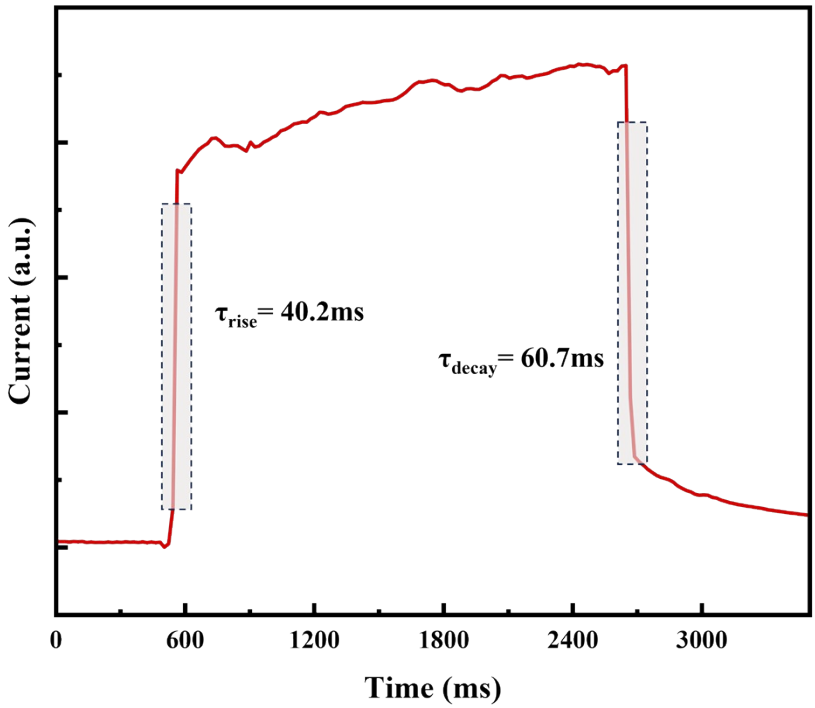

Fig. S7. Response time of the Planar reference structured PDs.

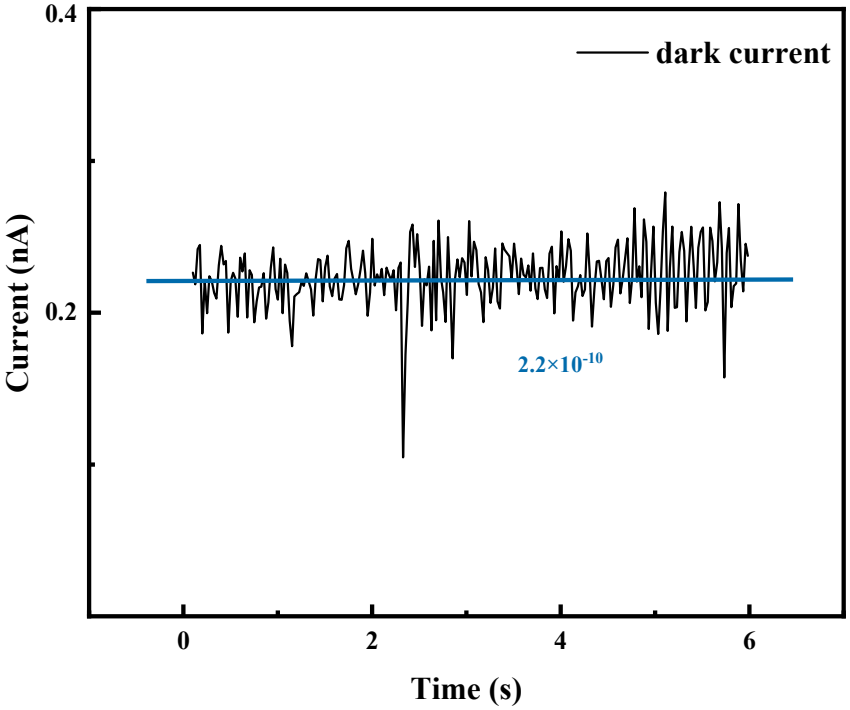

Fig. S8. Dark current of Dual-nanograting structured PDs.

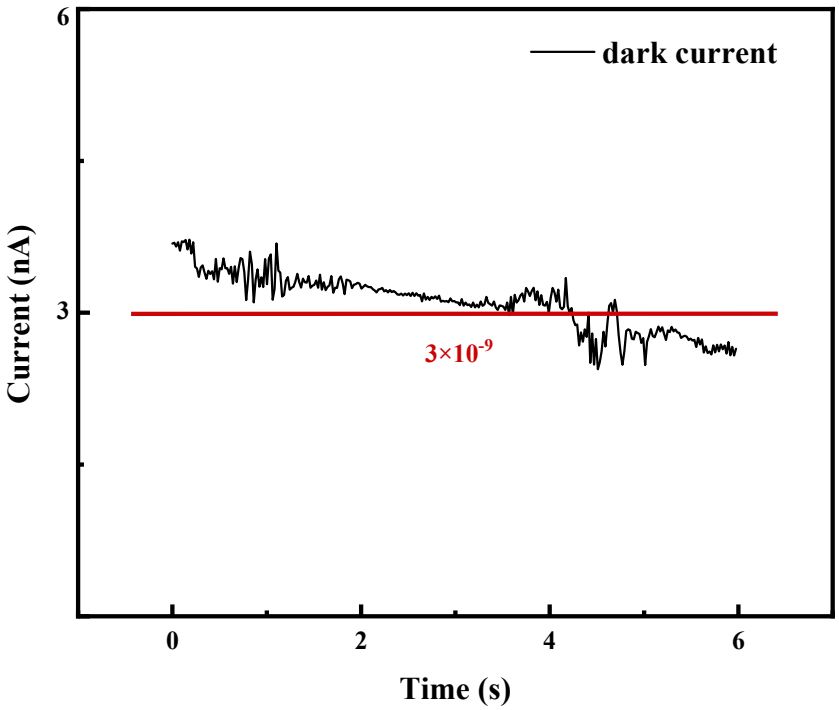

Fig. S9. Dark current of Planar reference structured PDs.

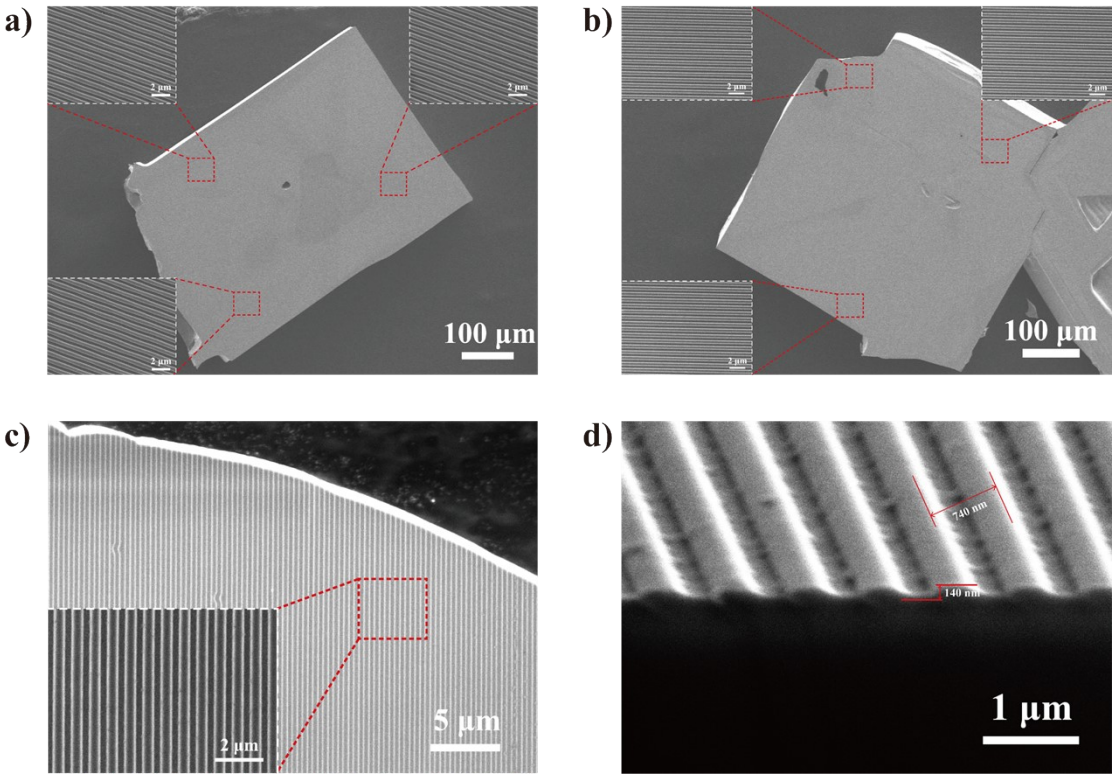

Fig. S10. SEM images of $MAPbBr_3$ crystals with DVD-template-derived surface gratings: (a, b) low-magnification views with enlarged insets; (c) enlarged edge region; (d) high-magnification grating profile showing a ~740 nm period and ~140 nm height difference.

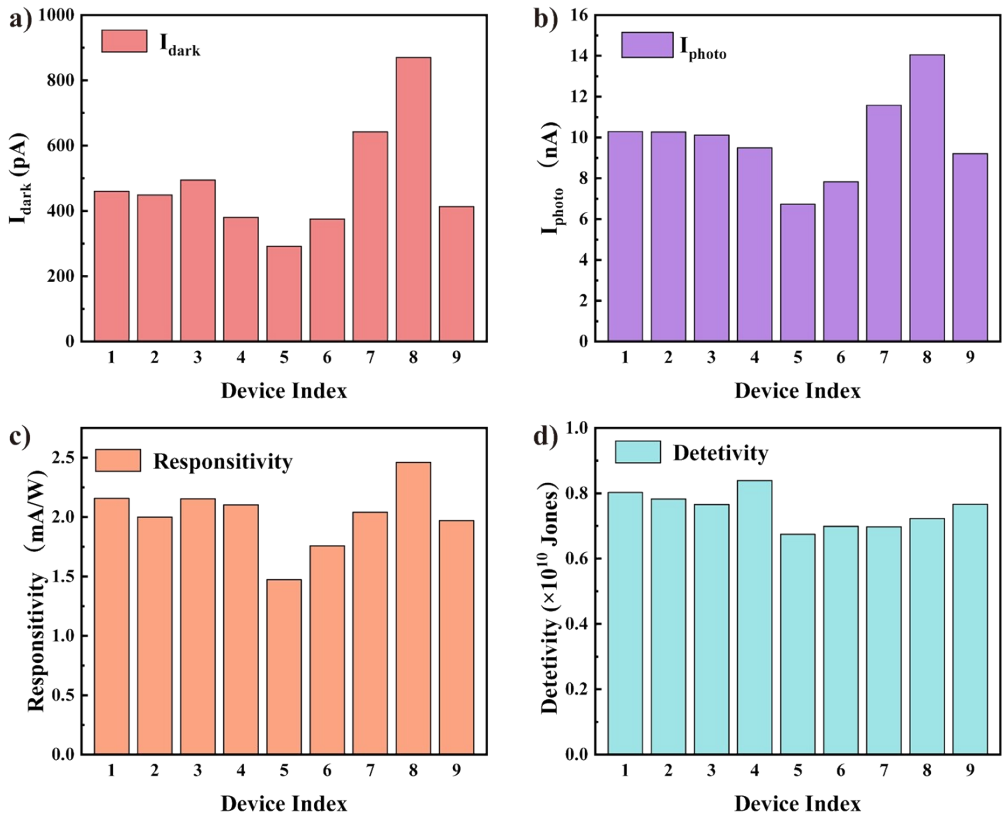

Fig. S11. Device-to-device performance statistics of DVD-template-derived Dual-nanograting photodetectors measured under identical conditions: (a) I_{dark}, (b) I_{photo} (c) responsivity, and (d) specific detectivity for devices fabricated at different positions (device index as the x-axis).

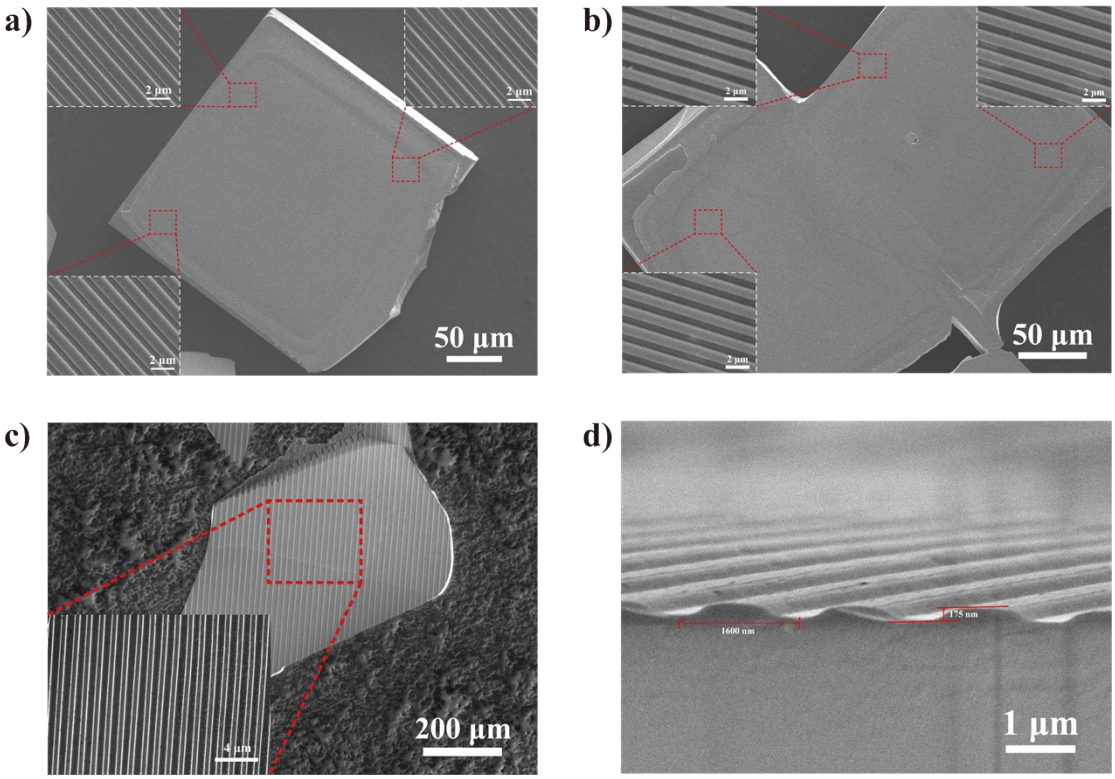

Fig. S12. SEM images of $MAPbBr_3$ crystals with CD-template-derived surface gratings: (a, b) low-magnification views with enlarged insets; (c) enlarged grating area; (d) high-magnification grating profile showing a ~1600 nm period and ~175 nm height difference.

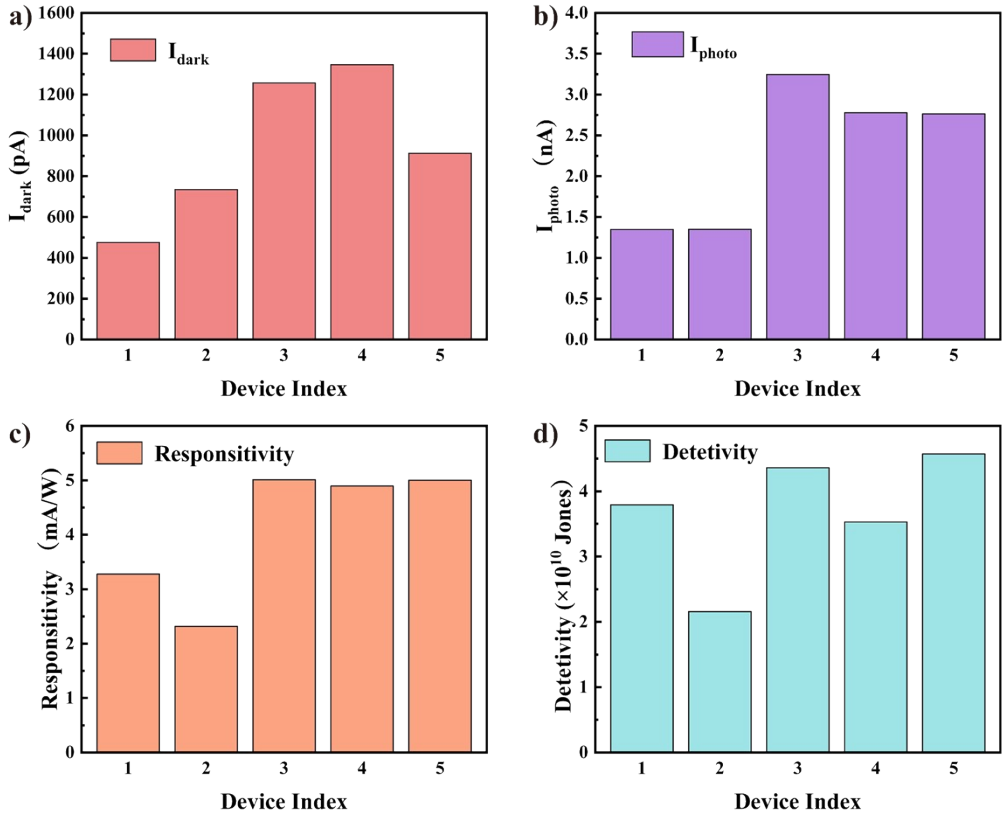

Fig. S13. Device-to-device performance statistics of CD-template-derived Dual-nanograting photodetectors measured under identical conditions: (a) I_{dark}, (b) I_{photo} (c) responsivity, and (d) specific detectivity for devices fabricated at different positions (device index as the x-axis).

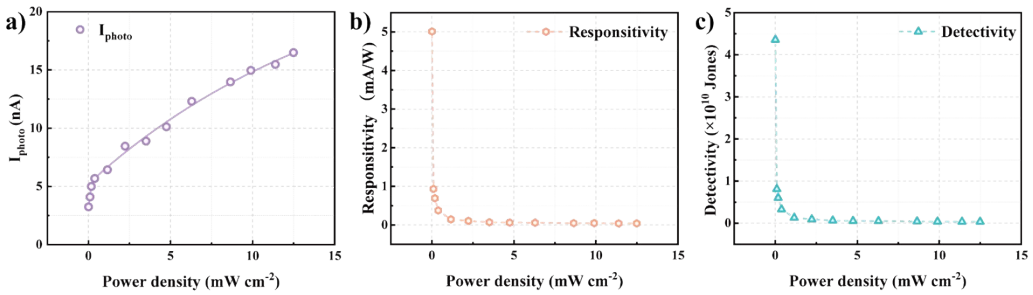

Fig. S14. Photoresponse and performance metrics of the CD-template-derived grating-structured devices under 365 nm illumination: (a) photocurrent, (b) responsivity, and (c) specific detectivity as a function of incident power density.

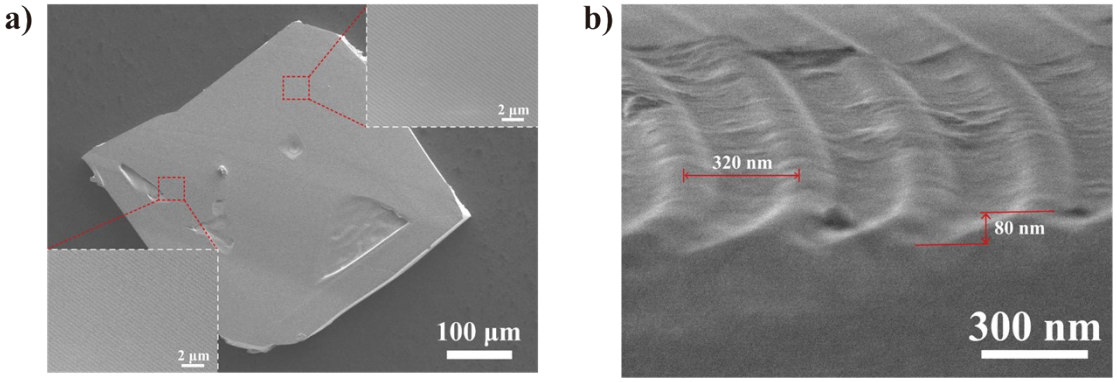

Fig. S15. SEM images of $MAPbBr_3$ crystal with BD-template-derived surface gratings: (a) low-magnification view with enlarged insets; (b) high-magnification grating profile showing a ~320 nm period and ~80 nm height difference.

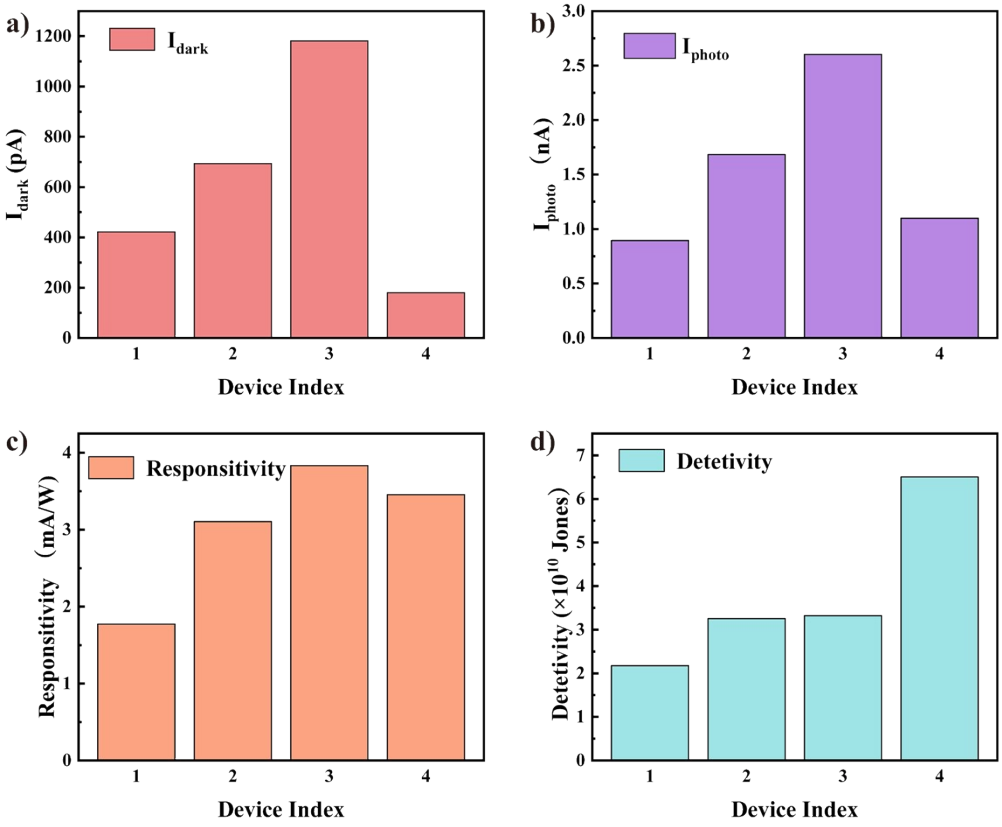

Fig. S16. Device-to-device performance statistics of BD-template-derived Dual-nanograting photodetectors measured under identical conditions: (a) I_{dark}, (b) I_{photo} (c) responsivity, and (d) specific detectivity for devices fabricated at different positions (device index as the x-axis).

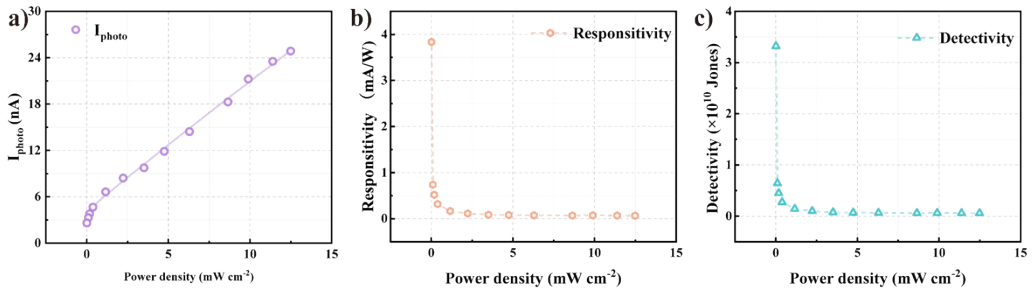

Fig. S17. Photoresponse and performance metrics of the BD-template-derived grating device under 365 nm illumination: (a) photocurrent, (b) responsivity, and (c) specific detectivity as a function of incident power density.

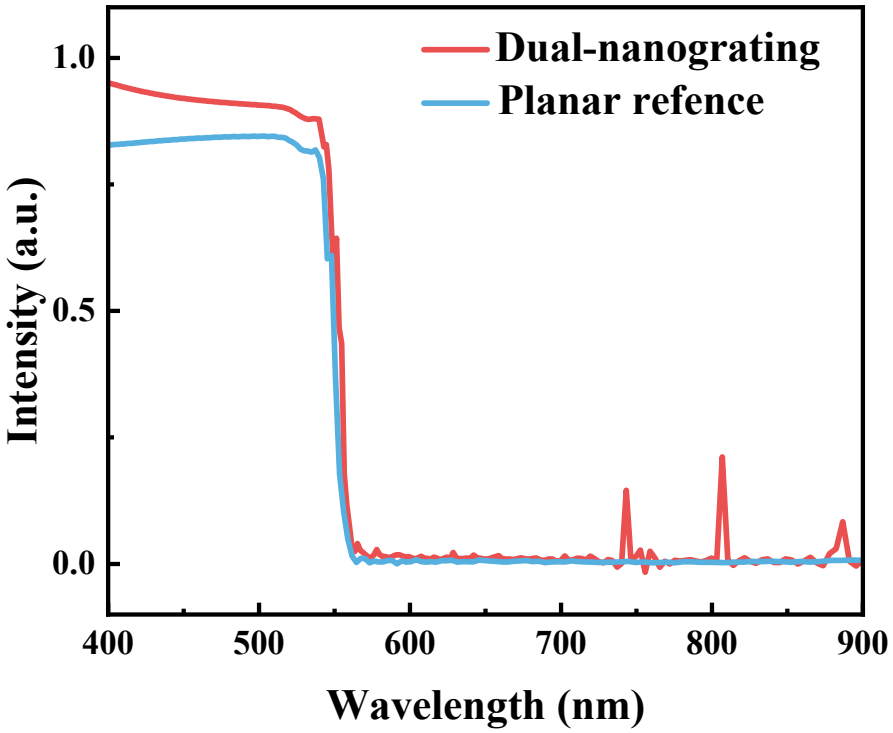

Fig. S18. FDTD-simulated absorption spectra of the Dual-nanograting and Planar reference. structures.

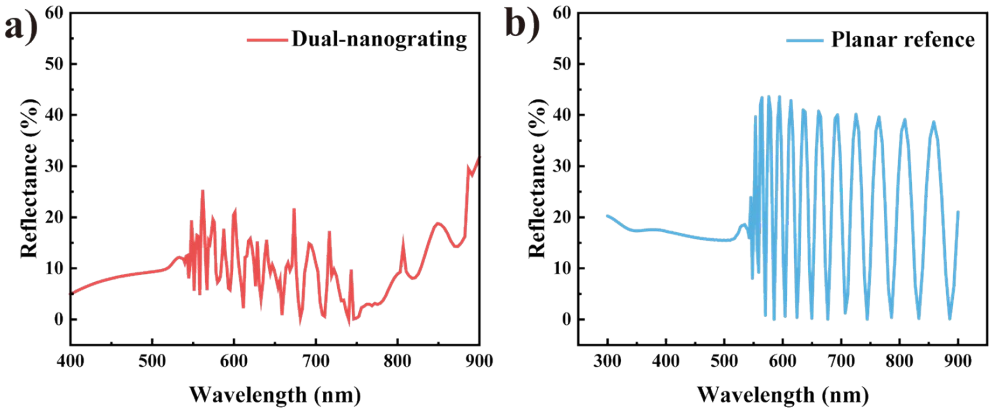

Fig. S19. FDTD-simulated reflectance spectra: (a) Dual-nanograting, (b) Planar reference.

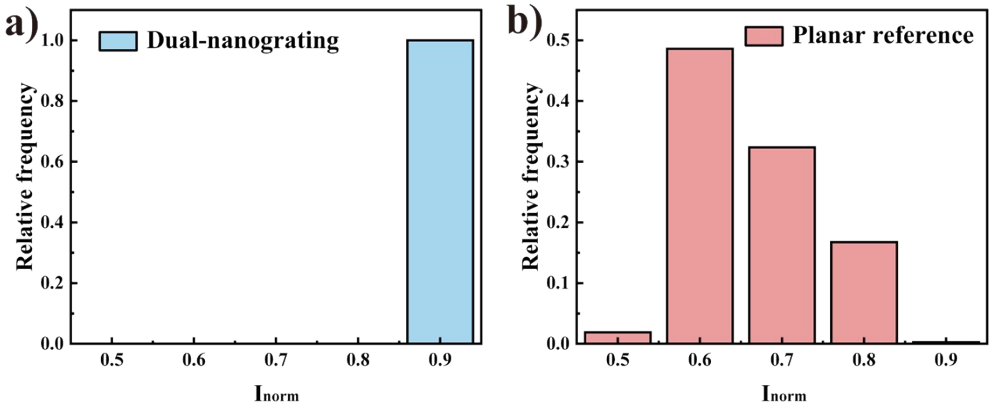

Fig. S20. Relative-frequency distribution of the normalized current I_{norm} over 800 switching cycles, showing the occurrence ratio of different normalized current levels: (a) Dual-nanograting device, (b) Planar reference. device.

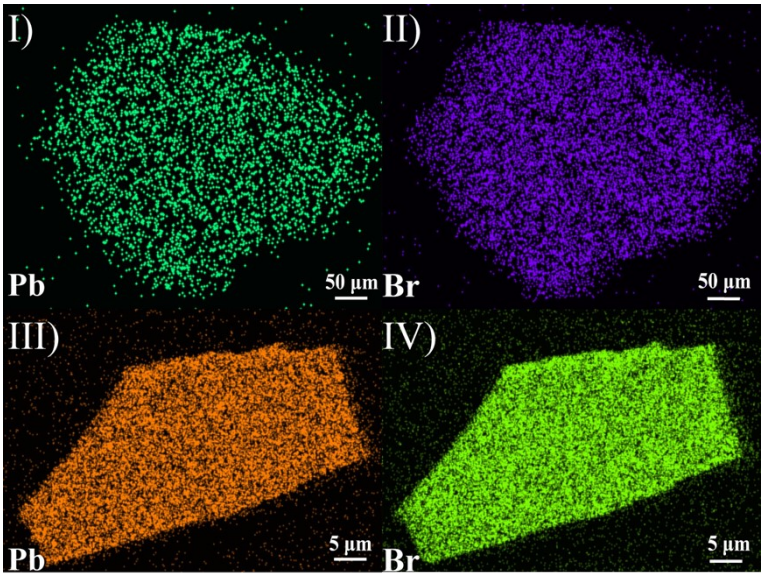

Fig. S21. Pb and Br distribution mapping of the crystal $MAPbBr_3$.

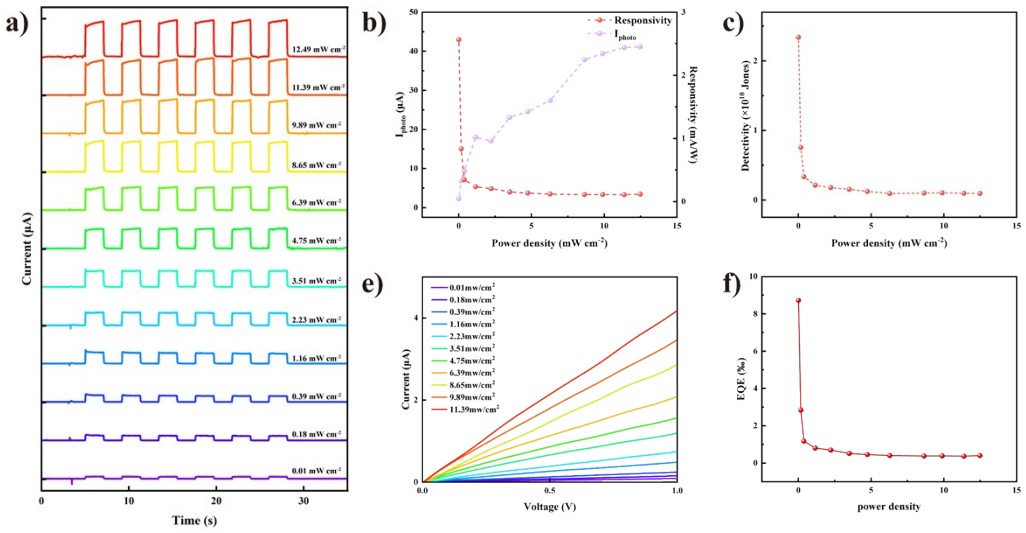

Fig. S22. Performance of the Planar reference perovskite photodetector under 365 nm light of varying intensity. (a) I–t curves. (b) Photocurrent and responsivity. (c) Specific detectivity. (d) I–V curves. (e) EQE.

Table S1. Comparison of photodetection performance of $MAPbBr_3$ Single-Crystal and Related Photodetectors

Materials	Wavelength (nm)	Bia (V)	R (mA W^{-1})	D^* (Jones)	EQE (%)	References
$MAPbBr_3$	**365**	**0.5**	**5**	**3.96×10^{10}**	**1.9**	**This work**
$MAPbBr_3$	570	-4	—	2×10^{10}	—	[1]
$MAPbBr_3$	525	5	1.54	6.02×10^{10}	—	[2]
$MAPbBr_3$	532	-1	0.394	1.10×10^{9}	—	[3]
$MAPbBr_3$	630	5	1.7	—	0.22	[4]
$MAPbBr_3$ (Au NPs)	630	5	2.4	—	0.37	[4]
ITO/$(PEA)_2PbI_4$/Au	475	10	0.75	2.76×10^{8}	0.17	[5]

1. Y. J. Fang, Q. F. Dong, Y. C. Shao, Y. B. Yuan and J. S. Huang, *Nat. Photonics*, 2015, **9**, 679-686.
2. H. Chen, C. Liu, P. Lin, H. H. Hu, Q. Y. Meng, L. B. Xu, P. Wang, X. P. Wu and C. Cui, *J. Alloys Compd.*, 2023, **935**, 8.
3. S. Y. Guo, S. Qiao, J. H. Liu, J. K. Ma and S. F. Wang, *Opt. Express*, 2022, **30**, 11536-11548.
4. Z. Q. Zhang, K. Chen, W. Xia and Z. Y. Zuo, *Mater. Res. Express*, 2020, **7**, 8.
5. Y. F. Yue, M. Y. Li, H. Li, N. Y. Chai, Y. F. Dong, Z. P. Li, X. Y. Chen and X. W. Wang, *Chem. Eng. J.*, 2022, **441**, 8.